Hindawi
Advances in Meteorology
Volume 2023, Article ID 6612199, 15 pages
https://doi.org/10.1155/2023/6612199

*Research Article*

# Spatiotemporal Variability of Hot Days in Association with the Large-Scale Atmospheric Drivers over Vietnam

**Chinh Ta Huu,[1] Tan Phan Van,[2] Khiem Mai Van,[3] Thang Vu Van,[1] Lam Hoang Phuc,[3] Worapong Lohpaisankrit,[4] Quoc Bao Pham,[5] Trinh Trong Nguyen,[6] and Phong Nguyen Thanh[7,8]**

[1]*Vietnam Institute of Meteorology Hydrology and Climate Change, Hanoi, Vietnam*
[2]*Department of Meteorology and Climate Change, VNU University of Science, Hanoi, Vietnam*
[3]*Vietnam National Center for Hydrology Meteorology Forecasting, Hanoi, Vietnam*
[4]*Department of Civil Engineering, Faculty of Engineering, Khon Kaen University, Khon Kaen, Thailand*
[5]*Faculty of Natural Sciences, Institute of Earth Sciences, University of Silesia in Katowice, Będzińska Street 60, 41-200, Sosnowiec, Poland*
[6]*HUTECH University, 475A Dien Bien Phu Street, Binh Thanh District, Ho Chi Minh City, Vietnam*
[7]*Laboratory of Environmental Sciences and Climate Change, Institute for Computational Science and Artificial Intelligence, Van Lang University, Ho Chi Minh City, Vietnam*
[8]*Faculty of Environment, School of Technology, Van Lang University, Ho Chi Minh City, Vietnam*

Correspondence should be addressed to Phong Nguyen Thanh; phong.nguyenthanh@vlu.edu.vn

Received 24 February 2023; Revised 20 June 2023; Accepted 25 July 2023; Published 17 August 2023

Academic Editor: Anzhen Qin



The severe heatwaves and hot spells in Vietnam were observed more frequently in intensity and duration due to global warming and climate change impacts. The hot days and extreme summer events make the weather harsh and significantly affect human health and the environment. This study presents the spatiotemporal distribution of the number of hot days (NHDs) in Vietnam. The variability of NHD in seven climate subregions is also examined in association with the large-scale drivers. The European Center for Medium-Range Weather Forecasts (ECMWF) reanalysis version 5 (ERA5) data for the period 1981–2020 are used. Principal component analysis is also applied to the observed monthly NHD to obtain spatial patterns and time series. The results show that the NHD in the Highland and South subregions from March to May is linked with the subtropical high associated with decreased 500hPa-level vertical velocity (VV500). From May to June, the North and Central subregions seem related to deepening the Asiatic low and enhancement of southwest flows across the Indochina Peninsula. Finally, both increased southwest flows and decreased VV500 can partly contribute to the intensification of NHD in the North and Central subregions during July and August. The long trends of NHD are also examined. The results reveal that the increasing trends in NHD occur in most subregions, except for the Central Highland, and changing trends of NHD in June greatly contribute to the annual trend of NHD. Finally, the examinations with the El Niño-Southern Oscillation events show that NHD is significantly higher in El Niño events than in La Niña events in March and April for the Northwest, South Central, Central Highlands, and South, in May and June for all subregions, and in July and August for only the Red River Delta subregion. This suggests that ENSO can provide the potential for improving seasonal climate forecasts and mitigating natural disaster risks for the community.

## 1. Introduction

A heat wave (HW) is one of the weather/climate extremes which cause serious problems relating to human health [1–4] as well as damages to the economy and society [5]. In the US, the mortality rate rises up by 3.73% during HW events [6]. In Europe, the extreme HW event in 2003 resulted in approximately 70,000 deaths [3, 7]. According to a study conducted by Nguyen et al. [8], it is estimated that in Vietnam, cold and heat waves were responsible for 1.42% of total deaths during the period from 2003 to 2017. Besides, high-temperature extremes directly relate to wildfire [5] as well as psychological stress [9]. In recent decades, with the impacts of global warming, severe HW spells have occurred more frequently, in both intensity and duration, in many places over the world, such as central and southern Africa [10, 11], southern Australia [12–14], North America [15–17], Russia [18, 19], China [20, 21], and central and southern Europe [22–25]. In Vietnam, there have been numerous instances where the surface temperature has reached extreme values, surpassing previous records. For instance, two extremely hot spells were recorded in 2019 (June 3 to July 1 in the North and July 4 to 29 in the Central region). During these events, the values of maximum daily temperature at provinces (Nghe An, Ha Tinh, and Binh Dinh) at the central level were over 40.0°C, and the new record was 43.3°C [26]. Thus, there is a demand to enhance the understanding of HW features and physical mechanisms leading to HW events.

Previous studies have been devoted to identifying interannual variations and changing trends of HW in both past and future projections [17, 27–33]. The variations of HW events are associated with various large-scale climate variabilities, such as the El Niño-Southern Oscillation (ENSO) [31, 34], North Atlantic Ocean [35], Indian Ocean Dipole [36], intraseasonal oscillation [37], and Indian Ocean basin modes [38, 39]. In addition, the relations between HW events and synoptic atmospheric patterns were also explored in some previous studies (e.g., [15, 40]). The intensification of HW has been attributed to various factors, such as the Tibetan snow cover [20], western Pacific subtropical high [30], East Asian jet stream [41], atmospheric blocking [42], East Asian winter monsoon (EAWM), and South Asian summer monsoon (SASM) [43].

A few studies examined the variation of HW in the Indochina Peninsula (IP) in association with large-scale drivers [43, 44]. Lin et al. [44] illustrated that El Niño (La Liña) events in the preceding winter tend to intensify (reduce) HW in the IP in the spring and summer of the following year. Luo and Lau [43] revealed distinct controls of large-scale atmospheric circulation to HW in dry and wet seasons in the IP. In particular, the increased extreme temperature during the dry season is associated with anomalous cyclonic circulation and anomalous southwesterly, implying the weakening of the East Asia winter monsoon. On the other hand, the HW events occurring during the wet season are attributed to anomalous easterly flows over the IP or the reduction of South Asia summer monsoon. Although Luo and Lau [43] documented an understanding of possible causes of HWs over the IP, the identification of HW events on daily maximum temperature-averaged whole IP can be less useful when the spatiotemporal distribution of HW is inhomogeneous, particularly in Vietnam, which has distinct climate conditions among different subregions. The southwesterly flow transports rainfall and humidity to most of the IP from the Indian Ocean during the wet season but can cause dry and hot climatic conditions for Northern and Central Vietnam, located at the eastern part of Truong Son Mountain, due to the Foehn effect. Pham and Phan [45] mentioned the impacts of the Foehn effect on HW in Northern and Central Vietnam but without specific evidence. While Luo and Lau [43] suggested the weakening of South Asia summer monsoon and the strengthening of easterly flows intensify HWs over the IP in the wet season, which contradicts the point of Pham and Phan [45]. Thus, the research of Luo and Lau [43] may still have limitations in explaining the intensifying of HW in Vietnam. Therefore, studying and identifying the contributing factors to HW in Vietnam are crucial.

Few studies were conducted to elucidate underlying reasons [45] but without detailed evidence. This study thus aims to investigate the spatiotemporal variability of the number of hot days (NHD: a characteristic of HW, as defined in Section 2.2) in Vietnam and its associations with large-scale climate processes. The rest of the paper is organized as follows: Section 2 presents data and methods, and Section 3 describes the spatiotemporal distribution, the long trend of NHD, and its possible links with large-scale drivers. The conclusions and recommendations are presented in Section 4.

## 2. Materials and Methods

### 2.1. Description of the Study Area

*2.1.1. Geographic Location of the Study Area.* The study focuses on the mainland of Vietnam (Figure 1), which is narrow in the west-east direction but stretches in the north-south direction with a long coastline of more than 3,000 km. Vietnam's territory encompasses 332,000 $km^2$ of land and a vast sea area, along with thousands of islands scattered throughout the East Sea. The country's maximum width stretches to about 500 km from the eastern coastline to the western border and narrows down to approximately 50 km in some areas. Vietnam's climate is tropical and monsoon, and it falls under the Southeast peninsula of the European-Asian mainland, spanning across latitude 15°, entirely located within the Northern Hemisphere's tropic inner belt, heavily influenced by the East Sea [46].

The five main types of terrain in Vietnam are mountains, karst, valleys and mountainous hollows, sedimentary deltas, and beaches. The most notable of these are the mountains and sedimentary deltas. Vietnam has seven different types of mountainous terrain: high mountains over 2,500 meters high, mostly in the Northwest region; average mountains 1,500–2,500 meters high, mostly in the Northeast, Northwest, North Central, and South Central regions; low

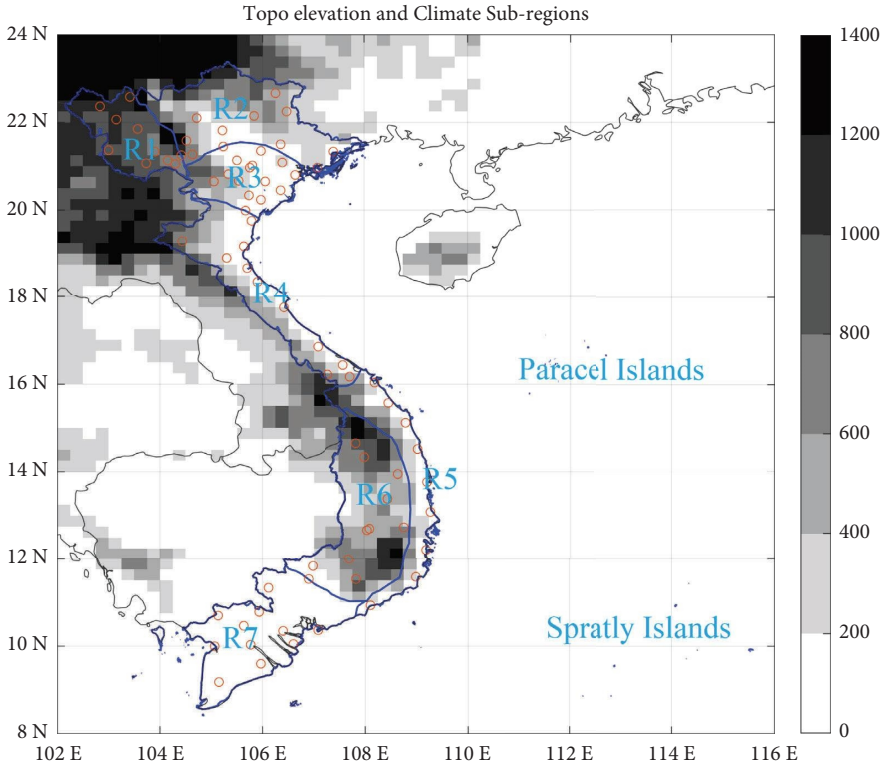


Figure 1: Seven climatic subregions with top elevator (meter: shading) are overlapped with the observed station network, including the Northwest (R1), Northeast (R2), Red River Delta (R3), North Central (R4), South Central (R5), Central Highlands (R6), and South (R7).

mountains 500–1,000 meters high, scattered across the nation; mountainous plateaus, mostly in the Central Highlands and Northwest regions; highlands focused in the Northwest regions; hills concentrated in the Northeast; and semiplains, which are normally found in the midland of the North and the South [46].

*2.1.2. Climate.* The Asian monsoon systems significantly impact Vietnam's climate, with the northeast monsoon occurring from November to April and the southwest monsoon from May to October. The country's complex topography, including high mountain ranges such as Hoang Lien Son in the North and Truong Son along the western border, is crucial in regulating these monsoons. These mountain ranges' directions are nearly perpendicular to the prevailing wind direction, leading to further complexity in the climate system. The climate of Vietnam is divided into seven subregions (Figure 1) or zones representing the climate based on geographical conditions [47]. The spatiotemporal variations of hot day numbers/heatwaves can also differ among subregions. The climatic regimes are totally different between the east (the Northeast, Central; R2–5) and west parts (the Central Highlands and South) of Truong Son Mountain. During the summer monsoon (May to October), the rainy season is in the Central Highlands and South, while the hot and dry conditions cover most of the Northeast, Central attributed to the existence of Truong Son. More details of features of hot days in Vietnam are represented in subsections 3.1 and 3.2.

*2.1.3. Soil.* According to data on soil categorization, Vietnam has 31 soil units and 14 major soil groupings [48, 49], in which there are three main soil groups: (1) mountainous soils, (2) hilly soils, and (3) delta soils. In mountainous and hilly regions, the predominant soil types are ferralitic soil (14.2 million hectares), acrisol, and alisol (also referred to as red soil for 3.1 million hectares). On the other hand, delta regions are mainly characterized by alluvial soils (3.4 million hectares), marine sandy soils (0.5 million hectares), and gley soils (0.5 million hectares) [50]. In the northern region of Vietnam, heavy rainfall during the season leads to the erosion of nutrient-rich topsoil from the highlands. This leaves behind slowly dissolving aluminum and iron oxides, resulting in the characteristic red hue of the soil. The land in the Red River Delta is diverse, with some soils being highly fertile and ideal for intensive farming, while others lack soluble bases. Fluvisols constitute approximately 25% of the land area in the Southern region, mainly in the Mekong River delta, along with peat and mud soils. Gray podzolic soils are present in certain parts of the Central Highlands (Tay Nguyen) and terraced fields along the Mekong River. Rejuvenated soils, rich in black humus and honeycomb rocks, are common in the Central Highlands (Tay Nguyen) and the coastal plain. Regosols, which are soft and underdeveloped, and noncalcium brown soils are situated along the central coast of Vietnam.

*2.1.4. Vegetation.* Vietnam's varied climate and terrain support a wide range of vegetation development, with around 2,084 native species, including six major forest types

including evergreen and semideciduous broad-leaved forests, deciduous forests, bamboo and palms, coniferous forests, open broad-leaved forests, and scrub [49]. The forested soil area, including nonclosed forests, covers up to 14 million ha, of which 10 million hectares are natural forests and 4 million hectares are planted forests. Forests meeting national coverage standards occupy 13 million hectares, accounting for 42.02% of the country's land coverage [51]. Furthermore, three quarters of Vietnam's territory are hilly or mountainous, and vegetation distribution above 1,000 meters above sea level shows significant changes [52].

### 2.2. Data and Data Processing

*2.2.1. Sources and Methods of Data Collection.* This study uses the observed maximum daily temperature (Tmax) data at stations throughout Vietnam to identify NHD. There are approximately two hundred observational stations over entire Vietnam, many in high mountain regions with mostly no NHD. Furthermore, most stations in the Southern part were established after 1976. Therefore, the daily Tmax data are collected from only the seventy-seven selected stations for the period 1981–2020 (40 years).

To examine the relationship between NHD and atmospheric circulation, the ERA5 reanalysis data (https://cds.climate.copernicus.eu/cdsapp#!/search?type=dataset) with a horizontal resolution of 0.25 degrees [53] of the monthly mean zonal (U925) and meridional (V925) wind at the 925 hPa level, the vertical velocity at 500 hPa (VV500 or Omega500), and the monthly mean sea level pressure (SLP) for the period 1981–2020 are used. UV925 and SLP are selected to depict the changes in monsoon regimes, such as northeasterly and southwesterly flows, and pressure centers (e.g., subtropical high and cold surge), respectively, while VV500 can reflect dynamic conditions at the midtropospheric level supporting/suppressing convection. In addition, the Niño-3.4 index obtained from the NOAA Prediction Center (https://psl.noaa.gov/data/climateindices/list/) was used to identify ENSO events.

*2.2.2. Data Quality Control.* Performing quality control on meteorological data in real time or soon after measurements is essential to minimize data loss [54]. This process involves identifying and correcting errors, checking for missing or incomplete data, and ensuring that the data meet the required standards and specifications to ensure accuracy, completeness, consistency, and reliability. In this study, the data provided by the National Center for Hydro-Meteorological Forecasting (NCHMF) and Vietnam Meteorological and Hydrological Administration (VNMHA) were through the quality control process.

*2.2.3. Heatwave and Hot Day Definition.* Since the hot day number is a characteristic of HW, we mention definitions of HWs before hot days. Some studies used relative thresholds, such as $90^{th}$ and $97.5^{th}$, a percentile value of daily maximum or mean temperature (e.g., [6, 30, 55–57]) during the historical period. An HW event is identified as two (or more) consecutive days having maximum (or mean) daily temperature equal to or greater than a specific threshold. Some other authors used absolute thresholds of daily Tmax as an indicator to determine HW. These thresholds are based on the local climate conditions. For example, Gao et al. [58] employed the daily Tmax threshold of 35°C combined with the relative humidity threshold of 60% to define HW days in China. In this study, we mainly focus on the NHD based on the regulation of the NCHMF in operational weather forecasting for Vietnam. Particularly, a hot day is defined as a day with daily Tmax equal to or greater than 35°C. An HW event is defined as a spell with at least two consecutive hot days (i.e., at least two consecutive days with daily Tmax equal to or greater than 35°C). Based on that, the NHD is identified as the total number of hot days of all HW events in a specific month/season/year.

*2.2.4. The Analysis Methods.* To examine the spatiotemporal variability of NHD, the annual and monthly means of NHD are calculated for each station and each climatic subregion. Besides, principal component analysis (PCA) [59, 60] is also applied for observed monthly NHD to obtain its spatial patterns (PCs) and time series (EOFs). The method can be briefly described as follows:

$$X(s,t) = \sum_{i=1}^{m} \mathrm{PC}_i(s)\mathrm{EOF}_i(t) \approx \sum_{i=1}^{k} \mathrm{PC}_i(s)\mathrm{EOF}_i(t), k \ll m, \tag{1}$$

where $X(s,t)$ is the data matrix of NHD, $t = 1, 2, \ldots, n$ is the time step (i.e., time series of the monthly NHD values), $s = 1, 2, \ldots, m$ is the number of stations, and $k$ is the number of dominant modes of the retained PCs. Particularly, $n = 40$ years $\times$ 12 months $= 480$ (months); $m = 77$ (stations).

The changing trend of NHD at each station is evaluated by nonparametric Sen's slope [61] and the Mann–Kendall test [62, 63] at a 95% confidence level. This approach has the advantage of not requiring any assumption on the data distribution. Besides, the Pearson correlation at a 95% confidence level (the percentage of times we expect to get close to the same estimate) is used to identify the link between NHD and the large-scale variables. The 95% confidence level is typically used to ensure that any observed trend is statistically significant and not simply due to chance.

Moreover, to examine the link between NHD and large-scale climate drivers, the correlation coefficients between EOFs and atmospheric circulation variables of U925, V925, VV500, and SLP are calculated. Besides, the differences in NHD during the ENSO events are also investigated. Impacts of ENSO on NHD are identified by the comparison of NHD during the strong El Niño (EN), La Niña (LA), and neutral (NU) years. A strong EN (LA) year is defined by the values of the Niño 3.4 index in December, January, and February greater (less) than 0.9°C (−0.9°C) [64, 65] and greater (less) than 0.5°C (−0.5°C) in March, April, and May. Based on that, seven EN years (1983, 1987, 1992, 1995, 1998, 2010, and 2016), seven LA years (1985, 1989, 1999, 2000, 2008, 2011,

and 2018), and nine NU years (1981, 1986, 1990, 1993, 1994, 2002, 2004, 2013, and 2014) have been selected.

## 3. Results and Discussion

*3.1. Spatiotemporal Variability of NHD.* Figure 2 shows the station-based annual and monthly total of NHD for the whole of Vietnam, while Table 1 presents the annual cycle of NHD for climatic subregions. It can be seen that hot days mainly occur from March to September. Thus, this study mainly focuses on NHD variability from March to September. In particular, the annual NHD is the highest in the North Central and South Central subregions, followed by the Northwest, Northeast, and Red River Delta, and the lowest numbers are in the Central Highlands and South (Figure 2(a)). The hot days start occurring the earliest over the Central Highlands and the South in March, followed by over the Northwestern and Central subregions in April, and then over the Northeastern and Red River Delta subregions in May (Figures 2(b)–2(h)). However, the hot days mostly occur in March–May over the Central Highlands and South, in May–September over the Northeast, Red River Delta, and Central, and in April–September over the Northwest. The occurrence of hot days in the Central Highlands and South is related to the dry season and apparent motion of the sun, which causes the high temperature and low humidity, while in the rest subregions, it could be attributed to the Foehn phenomenon. The early occurrence of hot days in the Northwest compared to the Northeast, Red River Delta, and Central might be associated with the activity of the Asiatic low during the early months of the Asian summer monsoon.

Figure 3 shows EOFs (time series) and corresponding PCs (spatial patterns) of NHD. It can be seen that the first two leading modes contribute 89.8% to the total variance. PC1 (65.5%) presents the dominant pattern of NHD over the Northwest, Northeast, Red River Delta, and Central subregions, while PC2 (24.3%) shows the dominant pattern of NHD over the rest parts of the country (i.e., Central Highlands and South subregions). Both PC1 and PC2 reveal negative values in the Northwest. EOF1 exhibits negative values in April, May, June, July, and August, reflecting the large values of NHD during these months, with the maximum in June, while EOF2 shows negative values in March, April, and May, with peaks in April.

It should be noted that, as described in (1), negative values in EOF1/EOF2 correspond to negative values in PC1/PC2, which leads to positive NHD. These results reflect the fact that the hot days in April and May can occur anywhere in the country. In general, the spatiotemporal variability of NHD is almost consistent with that presented in Table 1 and Figure 2. Although the features of NHD are distinct among subregions (e.g., numbers), they seem to be classified into two groups as described in EOF1 and EOF2. Also, using the EOFs to examine the link of NHD with large-scale drivers is feasible. Thus, the analysis of the underlying physical mechanism associated with NHD variability in subsection 3.4 is mainly based on the two first EOFs. Besides, applying PCA provides an overview analysis of NHD variability over Vietnam.

*3.2. Changing Trend of NHD.* Figure 4 shows trends of change in the annual and monthly NHD during 1981–2020, and Table 2 exhibits the maximum of Sen's slope over Vietnam. It is observed that the annual NHD significantly increased over most parts of the country (except for the South subregion), with the largest trend (1.5 days·year$^{-1}$, Table 2) in the Northeast, Red River Delta, and Central subregions. In these subregions, the increasing trend of NHD is largest in June, May, and September (around 0.5 days·year$^{-1}$ in June, Table 2). The NHD showed a significant increase in the Red River Delta subregion from May to September, followed by an increase in the Central. Meanwhile, the NHD significantly increased in the South in April and May. The lowest trend of NHD can be seen in the Central Highlands. The spatial pattern of NHD's trend in June is almost similar to that of the annual pattern (Figures 4(a) and 4(e)), implying that the change in NHD in June importantly contributes to the annual trend of NHD.

In general, the increase in NHD can be attributed to the increase in surface temperature. Nguyen et al. [66] analyzed surface temperature and rainfall variability in Vietnam during 1971–2010 based on the observed station data. The results show that the surface temperature tends to increase by 0.26°C per decade, and the increasing trends of temperature are higher in the winter than in the summer by 20–40%. The possible reasons for the increase in temperature are attributed to the enhancement of subsidence in the Hadley circulation around the latitudes of 10°N [66]. The fact that NHD increases significantly during May and June leads to the question of the underlying mechanisms that cause this surge. A future study will be conducted to investigate these mechanisms.

*3.3. Climatological Large-Scale Atmospheric Circulations.* Figure 5 depicts large-scale atmospheric circulation between 20°S and 40°N and 60 and 180°E throughout the climatological wind fields at 925 and 500 hPa levels. During March–April (MA), the IP and South China Sea (SCS) are driven by low-level northeasterly flows derived from cold surges (Figure 5(a)) as a component in the East Asia winter monsoon system around the latitudes of 35°N. At a higher level (500 hPa), the subtropical high-pressure system (STH) represented by the anticyclonic circulation between 10 and 20°N and 100 and 170°E (Figure 5(b)) around the Philippines Sea and southern SCS is active. During May and June (MJ), low-level southwesterly flows are a result of the association between those from the development of Asiatic low [66], and cross-equatorial flows are predominant over the IP and SCS (Figure 5(c)), while STH tends to move northward (Figure 5(d)). It should be noted that the transitional period among southwesterly and northeasterly monsoons over the IP is in late April and early May. It seems to be that July and August (JA) show the most active stage of southwesterly flows when they occupy most IP and SCS (Figure 5(e)). Simultaneously, STH moves to the latitudes of 25–30°N (Figure 5(f)), and southeasterly flows are at the southwestern flank of STH in association with cross-equatorial flows, resulting in the formation of an intertropical convergence

Table 1: Annual cycles (January–December) of NHD (day month$^{-1}$) in the climatic subregions (R1–R7) during the period 1981–2020.

| | Jan | Feb | Mar | Apr | May | Jun | Jul | Aug | Sep | Oct | Nov | Dec |
|---|---|---|---|---|---|---|---|---|---|---|---|---|
| R1 | 0.0 | 0.3 | 2.3 | 5.6 | 6.6 | 3.9 | 3.1 | 2.7 | 1.3 | 0.2 | 0.0 | 0.0 |
| R2 | 0.0 | 0.0 | 0.1 | 0.8 | 3.1 | 5.0 | 4.8 | 4.0 | 1.3 | 0.0 | 0.0 | 0.0 |
| R3 | 0.0 | 0.0 | 0.1 | 0.7 | 4.3 | 9.2 | 7.5 | 4.3 | 1.4 | 0.1 | 0.0 | 0.0 |
| R4 | 0.0 | 0.3 | 1.7 | 4.2 | 9.1 | 13.3 | 12.1 | 7.7 | 2.9 | 0.1 | 0.1 | 0.0 |
| R5 | 0.0 | 0.1 | 0.7 | 2.9 | 8.0 | 11.3 | 10.0 | 9.1 | 2.9 | 0.1 | 0.0 | 0.0 |
| R6 | 0.0 | 0.7 | 4.0 | 6.3 | 3.5 | 0.8 | 0.3 | 0.2 | 0.1 | 0.0 | 0.0 | 0.0 |
| R7 | 0.3 | 1.1 | 4.2 | 8.3 | 5.7 | 1.0 | 0.1 | 0.1 | 0.1 | 0.0 | 0.0 | 0.0 |

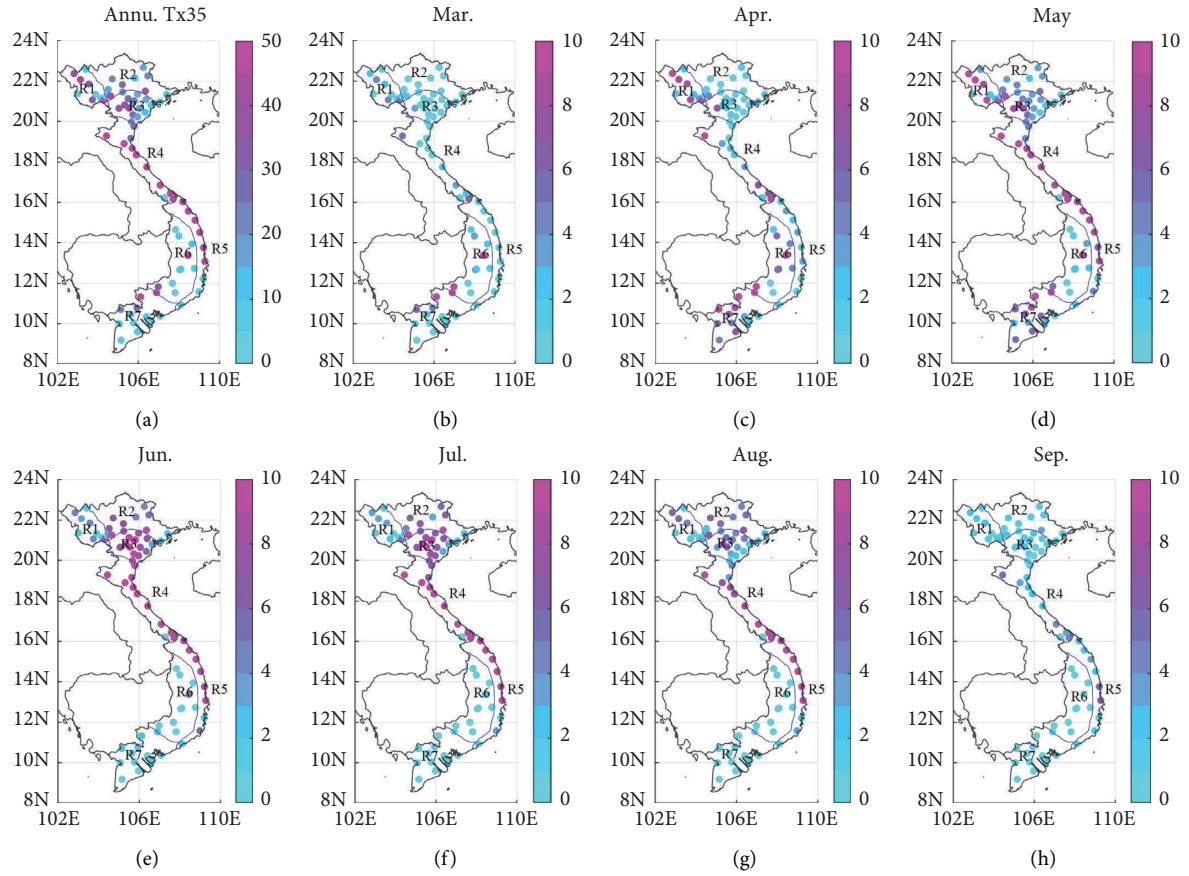


Figure 2: (a) The annual (day year$^{-1}$) and (b–h) monthly (for March–September, day month$^{-1}$) climatological values of NHD during the period 1981–2020. (a) Annu. T × 35. (b) March. (c) April.(d) May. (e) June. (f) July. (g) August. (h) September.

zone (ITCZ), which crosses and importantly contributes to rainfall regime over Vietnam, especially in the North and Central during July–November.

*3.4. Possible Links between Large-Scale Climate Drivers and NHD.* Figures 6–8 show the correlation coefficients between EOFs of NHD and corresponding atmospheric variables averaged for March-April (MA), May-June (MJ), and July-August (JA).

During March and April (MA), hot days mainly focus on the Northwest, Central Highlands, and South subregions (Table 1 and Figures 2 and 3). Thus, EOF1 (EOF2) mainly depicts NHD variability in the Northwest (the Central Highlands and South). It can be seen that the EOF1 of NHD has strong positive correlations with UV925 (Figures 6(a) and 6(c), the IP and the northern SCS) and strong negative correlations with SLP and VV500 (Figures 6(e) and 6(g), Northern Vietnam and China) over the area around 15–30°N, denoted as A1 area. Meanwhile, strong negative ones between EOF1 with UV925 (Figures 6(a) and 6(c), southern SCS, western North Pacific) and strong positive ones with SLP and VV500 (Figures 6(e) and 6(g), southern SCS, western North Pacific) gained over latitudes of 10°S–20°N are denoted as A2 areas.

As represented in Figure 5, climatologically, SCS and IP are governed by cold surges enhancing the dominance of northeasterly flows during MA. Thus, the positive (negative) correlations between EOF1 and UV925 (Figures 6(a) and 6(c)) can imply that the occurrence of hot days in the Northwest subregion is related to an anomalous anticyclone

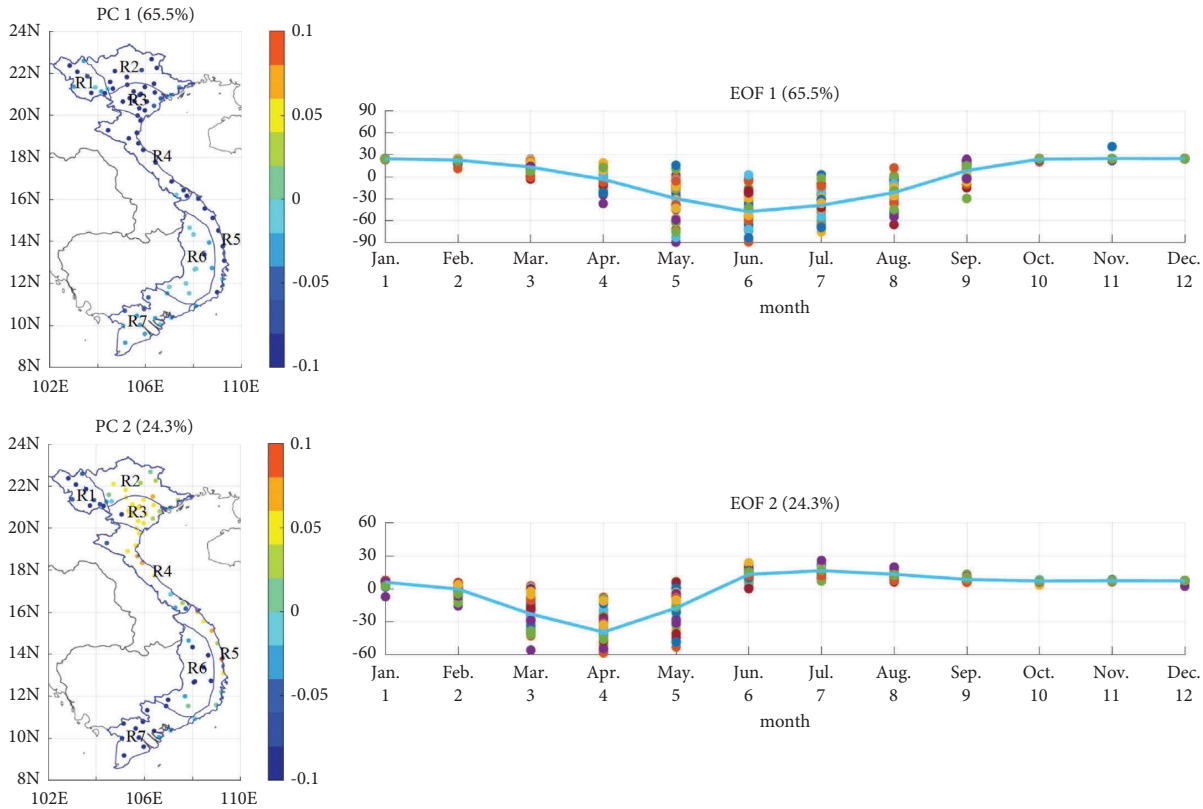


Figure 3: The first two leading modes of PCs and EOFs of NHD. Each dot (EOF time series) denotes the EOF value of a month in a year, and the solid line is the average of EOFs for each month.

Table 2: The maximum of Sen's slope (day year$^{-1}$) over Vietnam.

| Annu | March | April | May | June | July | August | September |
|---|---|---|---|---|---|---|---|
| 1.5 | 0.1 | 0.137 | 0.382 | 0.555 | 0.367 | 0.226 | 0.21 |

over SCS, which represents the weakening (enhancement) of northeasterly flows over A1 (A2). The negative correlations with SLP in the A1 area (Figure 6(e)) reflect the weaker activity of cold surges transporting cold and dry air masses from midlatitudes to the IP. Thus, the reduction of cold surges or anomalous northeast flows lead to a chance for intensification of temperature and hot days. On the other hand, positive ones with SLP in the A2 area (Figure 6(e)) represent the strengthening of subtropical high (STH). Thus, the weakening of cold surges and strengthening of STH can be considered as controlling factors to increasing NHD in the Northwest subregion. However, explaining the direct impacts of STH on NHD variability in the Northwest subregion is difficult. The simultaneous occurrence of the weakening of cold surges and the strengthening of STH can be considered a couple of patterns. Luo and Lau [43] also illustrated that the intensification of HW events in the IP during the dry season (November–April) is associated with anomalous cyclonic circulation over East Asia, contributing to the weakening of the East Asia winter monsoon.

The patterns of correlation between EOF2 of NHD and atmospheric variables in MA (right panels of Figure 6) are almost similar to those of EOF1, but with more intensification of the STH (Figures 6(b) and 6(f), also illustrated by further extension of anomalous easterly between 0 and 10°N to the Indian Ocean) in association with anomalous sinking flows (Figure 6(h), positive correlations with VV500 between 5 and 20°N) towards the IP. These patterns are associated with the occurrence of hot days in the Central Highlands and South. Luo and Lau [43] also demonstrated that the HW events in the IP are related to the decrease of vertical velocity and increase of geopotential height, which is consistent with the results in the current study.

The relationships between EOFs of NHD variability and atmospheric drivers in May and June (MJ) are presented in Figure 7, which are almost similar to those in MA, but large-scale atmospheric behaviors to NHD variability need to be explained in another way. Climatologically, during MJ, the Southwest wind dominates the whole IP, and the Asiatic low [66] is active instead of a cold surge at a low level. Therefore, the strong positive correlations with UV925 in A1 indicate the development of anomalous southwesterly flows across the IP and Vietnam. The strong negative correlations between EOF1 with SLP and VV500 (Figures 7(e) and 7(g)) over Southeast China and North Vietnam are linked with the strengthening of the Asiatic low favorable for enhancing anomalous southwesterly flows. Moreover, extending the strong negative correlation between EOF1 and U925 (Figure 7(a)) towards the Southern Hemisphere (latitudes of 10–20°S) can suggest the enhancement of the cross-

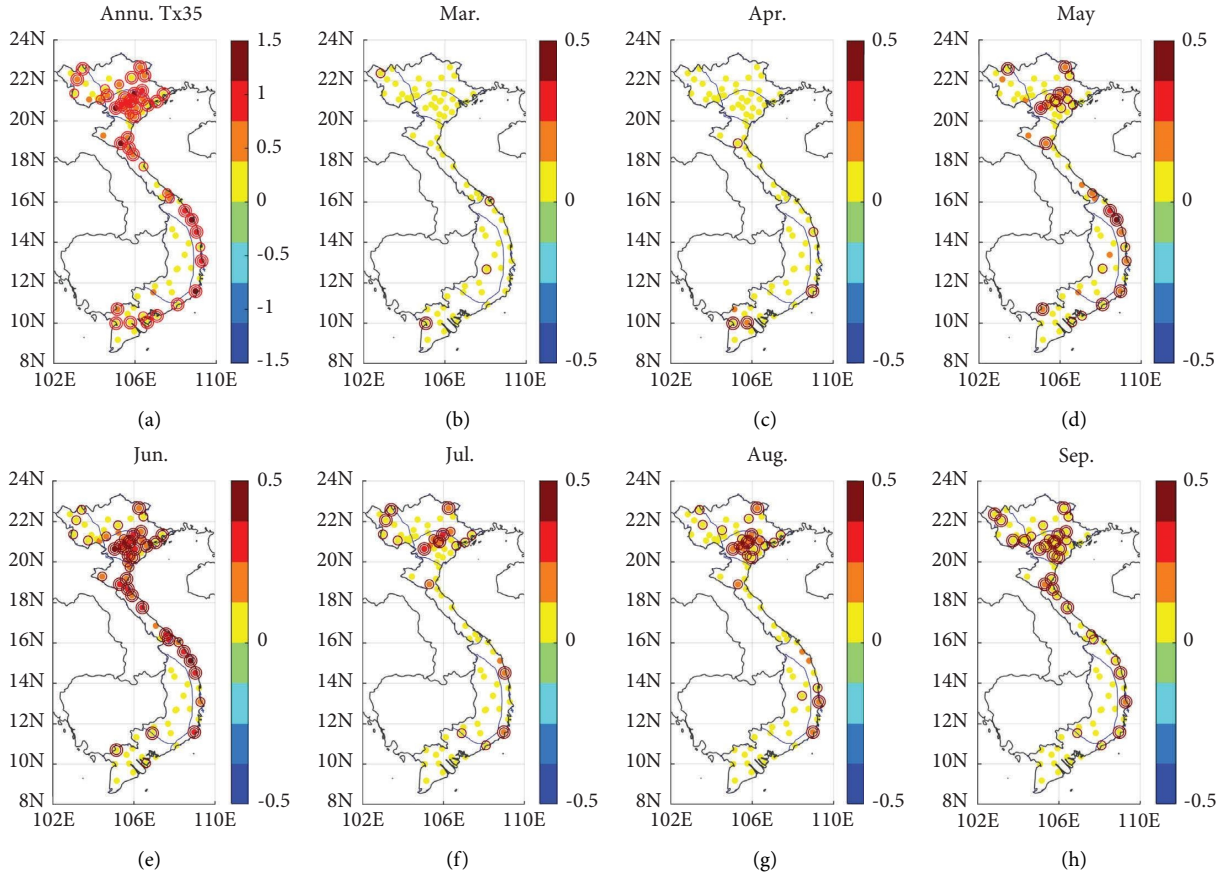


Figure 4: Sen's slope coefficients of NHD for annual (day year$^{-1}$) and months (day year$^{-1}$). The stations with a circle surrounding them are satisfied at a 95% confidence level. (a) Annu. T × 35. (b) March. (c) April.(d) May. (e) June. (f) July. (g) August. (h) September.

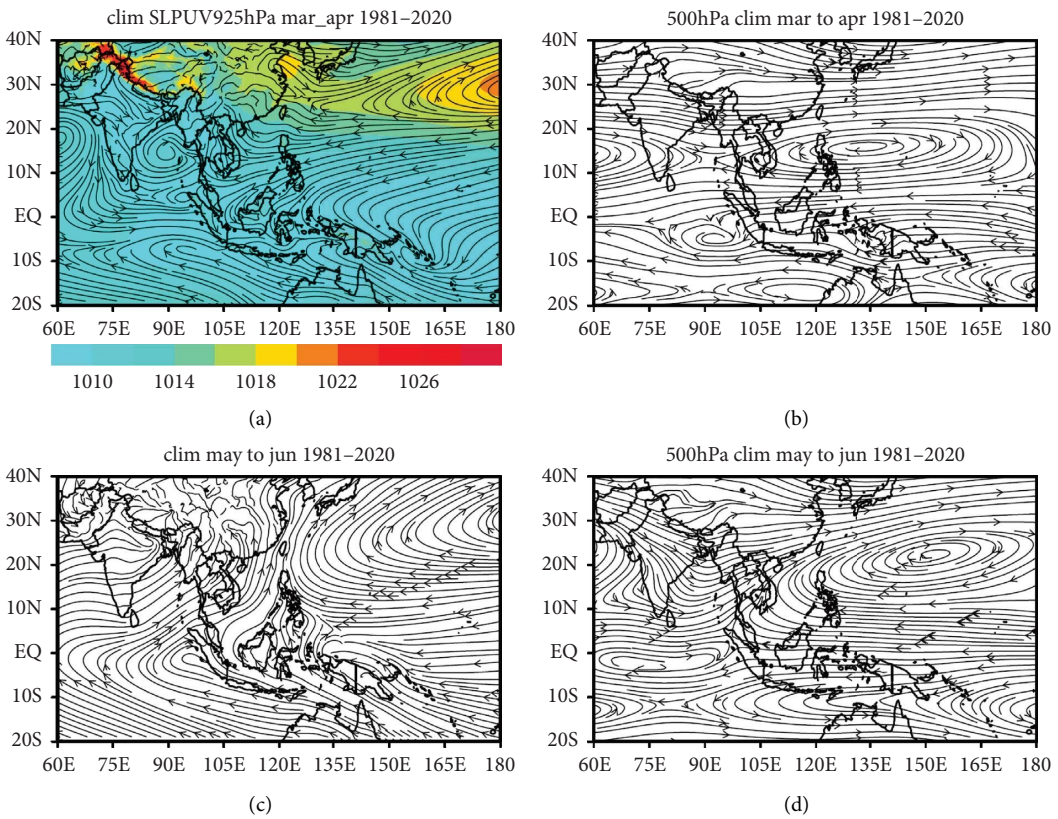


Figure 5: Continued.

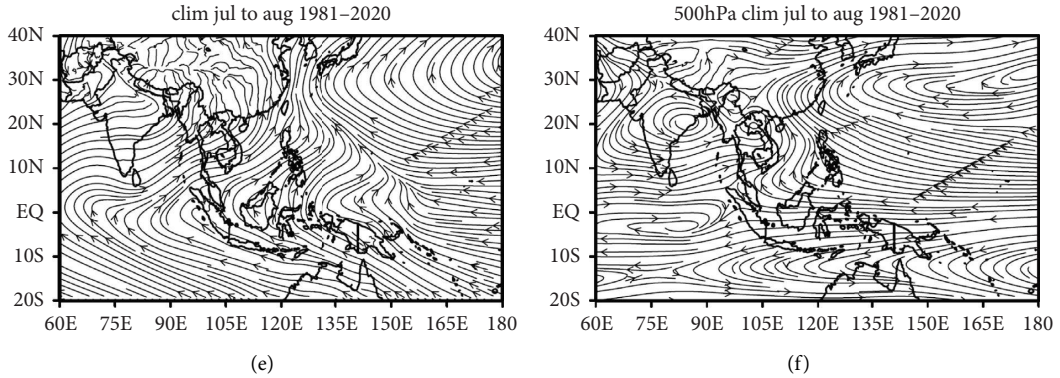


Figure 5: Climatological wind and sea level pressure fields averaged for 1981–2020 at 925 hPa (left) and 500 hPa (right): (a) sea level pressure (shading) overlapped with streamline and (b–f) streamlines. (a) Clim SLPUV925hPa mar_apr 1981–2020. (b) 500hPa clim mar to apr 1981–2020. (c) Clim may to jun 1981–2020. (d) 500hPa clim may to jun 1981–2020. (e) Clim jul to aug 1981–2020. (f) 500hPa clim jul to aug 1981–2020.

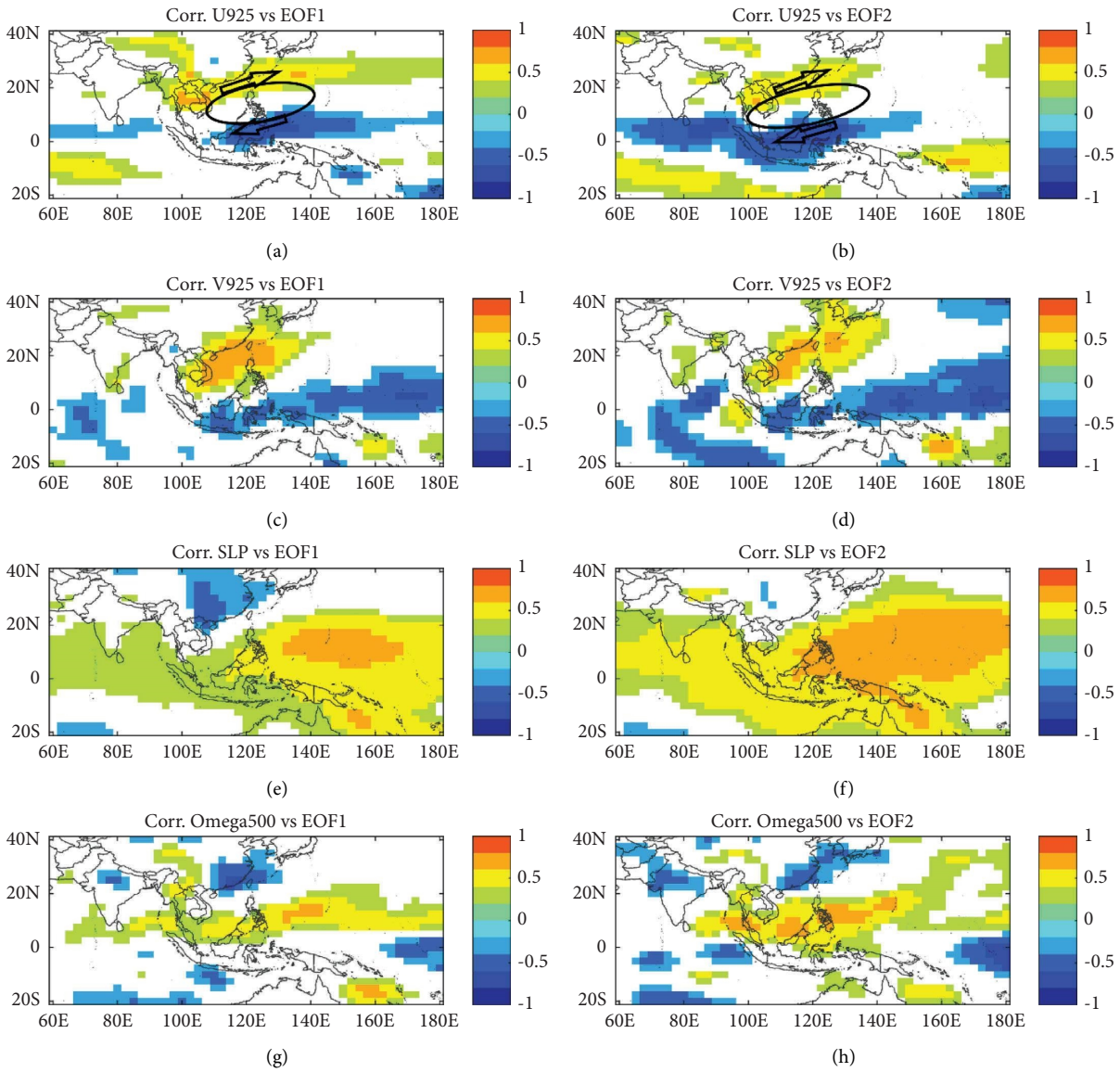


Figure 6: The correlations (at the 95% confidence level) between EOF1 of NHD vs. (a, c, e, g) atmospheric variables; similar to EOF2 (b, d, f, h) for March and April (MA). (a) Corr. U925 vs. EOF1. (b) Corr. U925 vs. EOF2. (c) Corr. V925 vs. EOF1. (d) Corr. V925 vs. EOF2. (e) Corr. SLP vs. EOF1. (f) Corr. SLP vs. EOF2. (g) Corr. Omega500 vs. EOF1. (h) Corr. Omega500 vs. EOF2.

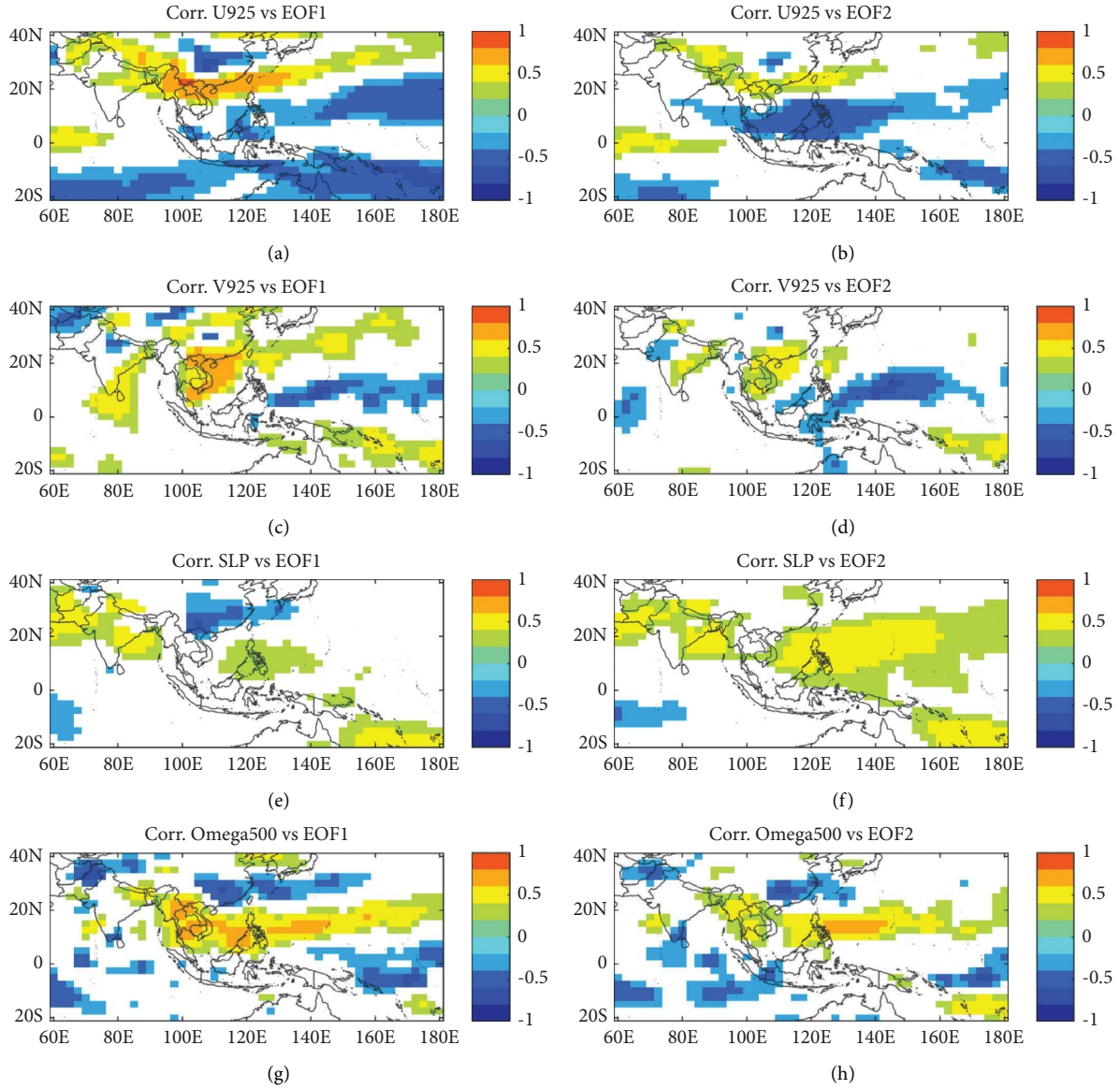


Figure 7: Same as Figure 6 but for May-June (MJ). (a) Corr. U925 vs. EOF1. (b) Corr. U925 vs. EOF2. (c) Corr. V925 vs. EOF1. (d) Corr. V925 vs. EOF2. (e) Corr. SLP vs. EOF1. (f) Corr. SLP vs. EOF2. (g) Corr. Omega500 vs. EOF1. (h) Corr. Omega500 vs. EOF2.

equatorial flows from the Southern Hemisphere's STH. Besides, strong positive correlations with VV500 extending and covering most of the IP (Figure 7(g)) implicate decreased VV500. These patterns lead to the intensification of NHD in the North and Central subregions. Pham and Phan [45] mentioned the effects of the Foehn winds (southwesterly flows) on distinct climate regimes among windward (Laos and Cambodia) and leeward sides (the Northeast, Red River Delta, and Central Vietnam) of Truong Son mountain. Most of the moisture and rainfall in the southwesterly summer monsoon is dropped out on the windward side, and hot, dry air is retained on the leeward side in the Northeast, Red River Delta, and Central subregions of Vietnam. Nguyen et al. [66] evidenced a distinction in the convective activity between the windward and leeward sides of Truong Son Mountain through changes in relative humidity and outgoing longwave radiation. Thus, the results from the current study suggest direct and additional roles of low-level anomalous southwesterly flows (the Foehn wind) and midtropospheric level anomalous vertical velocity at 500 hPa to NHD intensification, respectively. Similar to the pattern of EOF2 in MA, the correlations between EOF2 and UV925, SLP, and VV500 (Figures 7(b), 7(d), 7(f), and 7(h)) in MJ depict controlling factors of NHD intensification over the Central Highlands and South subregions, such as the strengthening of STH, and the decrease in VV500. Besides, the results also represent stronger and weaker anomalous westerly flows over 17–22°N and 0–17°N (Figures 7(b)), respectively, which can link with the northward movement of STH, respectively, compared to MA. On the other hand, it is also displayed by strong positive correlations with SLP between latitudes of 0–20°N in Figure 7(f).

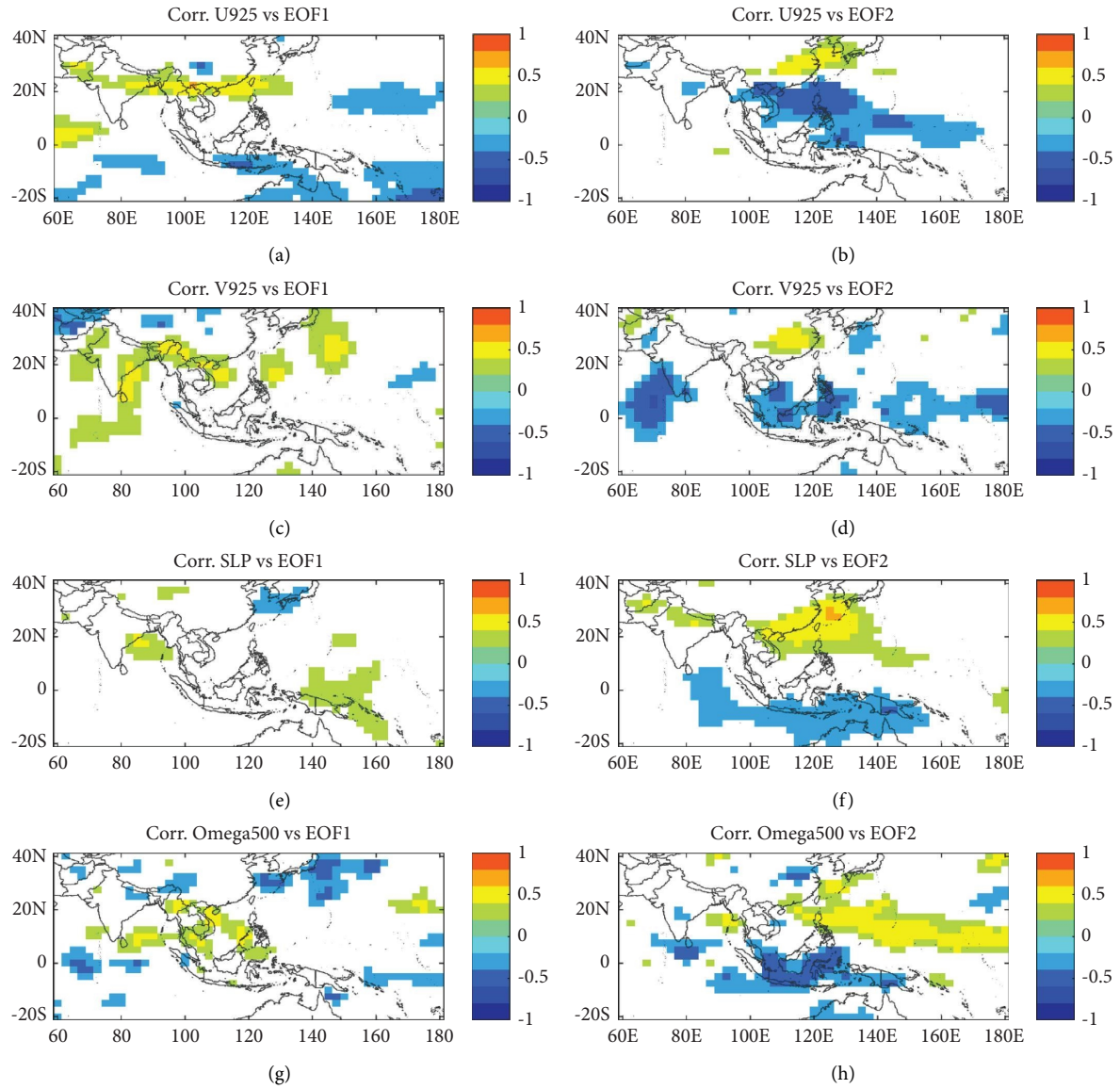


Figure 8: Same as Figure 6 but for July-August (JA). (a) Corr. U925 vs. EOF1. (b) Corr. U925 vs. EOF2. (c) Corr. V925 vs. EOF1. (d) Corr. V925 vs. EOF2. (e) Corr. SLP vs. EOF1. (f) Corr. SLP vs. EOF2. (g) Corr. Omega500 vs. EOF1. (h) Corr. Omega500 vs. EOF2.

The variability of NHD in the southern regions of Vietnam (Central Highlands and South) appears to be more influenced by anomalous easterly flows than in the North and Central regions. Luo and Lau [43] demonstrated that HW events over the IP in the wet season are associated with the weakening of the South Asia summer monsoon and the strengthening of easterly flows, which is consistent with the mechanism over the Central Highlands and South Vietnam but is opposite of that over the North and Central Vietnam. It can be explained that the plains of North and Central Vietnam are totally different from other areas of the IP in climate regimes due to the existence of Truong Son Mountain (e.g., the Foehn winds). Thus, the controlling factors for NHD variability are not the same. Moreover, the HW events in Luo and Lau [43] are averaged for the whole IP, missing the climatic features over the small and narrow plains as in North and Central Vietnam.

Similarly, Figure 8 displays the moderate correlations between the NHD variability of JA and corresponding atmospheric variables. Note that during JA, the NHD appears in the Northeast, Red River Delta, and Central, mainly represented in EOF1 (65% of total variance), although EOF2 also depicts a small fraction of NHD variability. The patterns of the moderate positive correlations with UV925 (Figures 8(a) and 8(b)) in EOF1 exhibit the increase of NHD over the North and Central in response to the intensification of anomalous southwest flows. Simultaneously, the moderate correlations with VV500 show decreased vertical velocity in the North and Central (Figure 8(g)). Meanwhile, EOF2 presents an opposite pattern with the intensification of SLP between latitudes of 15 and 35°N (moderate positive correlations with SLP, Figure 8(f)), followed by the development of anomalous southeasterly flows (moderate negative correlations with

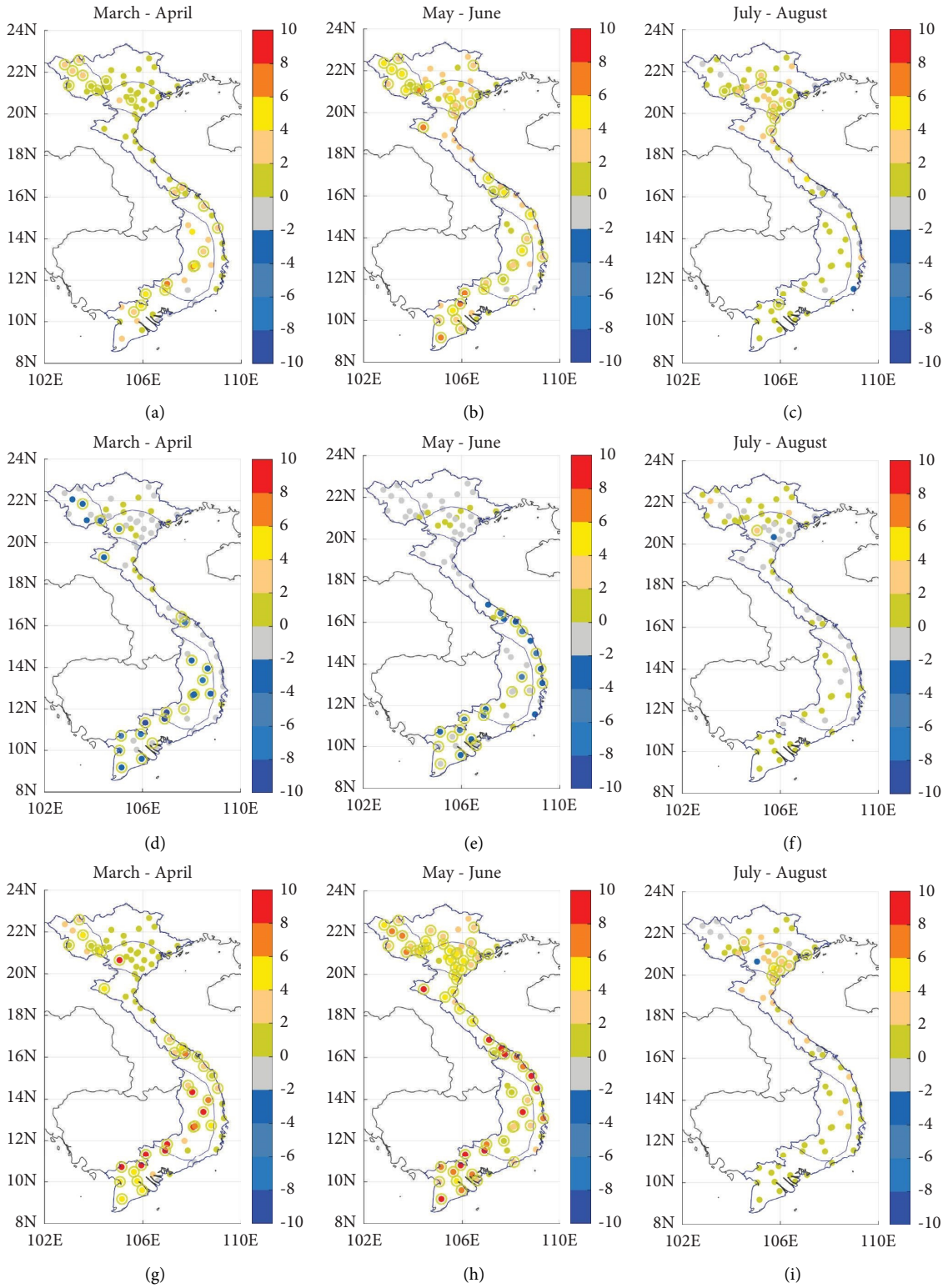


Figure 9: Differences of NHD between (a–c) EN and NU years, (d–f) LA and NU years, and (g–i) EN and LA years. The dots with circles are at a 95% confidence level. (a) March-April. (b) May-June. (c) July-August. (d) March-April. (e) May-June. (f) July-August. (g) March-April. (h) May-June. (i) July-August.

UV925, Figures 8(b) and 8(d)) towards North and Central Vietnam.

The intensification of SLP and anomalous southeasterly flows towards Northern Vietnam implies the westward extension of STH (compared to the climatology of STH in Figure 5). Simultaneously, the decrease of VV500 (positive correlations with VV500, Figure 8(h)) expanding from the SCS to the Philippines Sea can exhibit the weakening of ITCZ (compared to the climatology), suppressing convection and rainfall to enhance NHD over the North and Central. Therefore, the analysis shows that during JA, the increasing NHD in the North and Central subregions is mainly related to controls of low-level anomalous southwesterly flows, decreasing vertical velocity over Northern and Central Vietnam, and a fraction from STH is in association with the weakening of ITCZ and active southeasterly flows.

Figure 9 shows the differences in NHD between EN and NU years (Figures 9(a)–9(c)), LA and NU years (Figures 9(d)–9(f)), and EN and LA years (Figures 9(g)–9(i)) for the months of March-April, May-June, and July-August. It can be seen that the NHD is higher (lower) in EN (LA) years than in NU years during MA, MJ, and JA, especially in MA and MJ. Significant positive differences in NHD between EN and NU years occur in MA over the Northwest, Central, Central Highlands, and South subregions and in MJ over the Northwest, Red River Delta, South Central, Central Highlands, and South subregions. The positive differences in NHD between EN and LA years have the same pattern as those between EN and NU years, but the values are much larger. The NHD is significantly higher in EN years than in LA years in MA for the Northwest, Central Highlands, and South subregions, MJ for almost all countries, and JA for the Red River Delta subregion.

Some previous studies illustrated the intensification of HW in EN events compared to LA events in the IP. The study of Lin et al. [44] found that the development of EN (LA) events in the preceding winter tends to enhance (weaken) the HWs in the IP. It can be explained by an occurrence of an anomalous sinking motion over the western north Pacific (WNP) and Asia during EN events, leading to suppressed precipitation and enhanced HWs [43, 44]. Some authors demonstrated that anomalous anticyclonic circulation, as shown in Figures 6(a) and 6(b), is formed in the Philippines Sea during EN events [67, 68].

## 4. Conclusion and Recommendations

This study examines the spatiotemporal variability of NHD over Vietnam in association with the large-scale climate drivers. The results show that NHD in the Central Highlands and the South subregions occur from March to May. Other subregions seem to share the annual cycles of NHD from May to September. Yet, NHD in the Northeast, Red River Delta, and Central of Vietnam generally peaks in June and July, while that in the Northwest peaks between April and May. Besides, the increasing trends in NHD occur in most subregions, except for the Central Highlands. Interestingly, it seems that the changing trends in June greatly contributed to the annual trend.

The intensification of NHD in the Central Highland and the South subregions in March–May is related to the westward extension of STH towards the IP in association with decreased VV500, while that in the Northwest in April is driven by the weakening of northeast flows. The intensification of NHD in the North and Central during MJ is linked with the strengthening of Asiatic low pressure and anomalous southwest flows, leading to the Foehn effects caused by the Truong Son Mountain range. Finally, the peak of NHD in the North and Central of JA is partly controlled by the southwest flows. Besides, the decreased vertical velocity in the midtropospheric level, which can be related to the weakened ITCZ, also contributes to NHD at these subregions. Further examinations of NHD concerning ENSO show that the NHD is significantly higher in EN events than in LA events in MA for the Northwest, South Central, Central Highlands, and South, in MJ for all subregions, and in JA for only the Red River Delta subregion.

The present study contributes to a better understanding of the relationship between large-scale circulation and NHD variability in Vietnam. However, it still has certain limitations, such as the lack of an explanation for the NHD increase in June or the underlying causes of NHD variability in September, which may differ from those in July and August. These issues will be addressed in future studies. Furthermore, the study findings suggest that ENSO indices, such as El Niño 3.4, could be potential predictors for seasonal forecasting of hot day numbers in Vietnam as well as to research to develop a seasonal prediction model for hot days based on sea surface temperature anomalies.

## Data Availability

The data used to support the findings of this study are available from the following hyperlinks: monthly large-scale atmospheric fields from the European Center for Medium-Range Weather Forecast (ECMWF) (https://cds.climate.copernicus.eu/cdsapp#!/dataset/reanalysis-era5-single-levels?tab=overview), observed data (daily maximum surface temperature) from NCHMF (https://thoitietvietnam.gov.vn/Kttv/vi-VN/1/index.html), and the El Niño 3.4 index obtained from the NOAA Prediction Center (https://psl.noaa.gov/data/climateindices/list/).

## Conflicts of Interest

The author declares that there are no conflicts of interest.

## Funding

This research was funded by research projects with codes: TNMT.2021.02.05, TNMT.2023.06.02, ĐTĐL.CN-119/21, and ĐTĐL.CN-90/21.

## References


[1] C. B. Field, V. Barros, T. F. Stocker, and Q. Dahe, *Managing the Risks of Extreme Events and Disasters to advance Climate Change Adaptation: Special Report of the Intergovernmental Panel on Climate Change*, Cambridge University Press, Cambridge, UK, 2012.

[2] G. A. Meehl and C. Tebaldi, "More intense, more frequent, and longer lasting heat waves in the 21st century," *Science*, vol. 305, no. 5686, pp. 994–997, 2004.

[3] J. M. Robine, S. L. K. Cheung, S. Le Roy et al., "Death toll exceeded 70,000 in Europe during the summer of 2003," *Comptes Rendus Biologies*, vol. 331, no. 2, pp. 171–178, 2008.

[4] M. Li, S. Gu, P. Bi, J. Yang, and Q. Liu, "Heat waves and morbidity: current knowledge and further direction-a comprehensive literature review," *International Journal of Environmental Research and Public Health*, vol. 12, no. 5, pp. 5256–5283, 2015.

[5] J. Zuo, S. Pullen, J. Palmer, H. Bennetts, N. Chileshe, and T. Ma, "Impacts of heat waves and corresponding measures: a review," *Journal of Cleaner Production*, vol. 92, pp. 1–12, 2015.

[6] G. B. Anderson and M. L. Bell, "Heat waves in the United States: mortality risk during heat waves and effect modification by heat wave characteristics in 43 US communities," *Environmental Health Perspectives*, vol. 119, no. 2, pp. 210–218, 2011.

[7] R. Garcıa-Herrera, J. Dıaz, R. M. Trigo, J. Luterbacher, and E. M. Fischer, "A review of the European summer heat wave of 2003," *Critical Reviews in Environmental Science and Technology*, vol. 40, no. 4, pp. 267–306, 2010.

[8] C. V. Nguyen, M.-H. Nguyen, and T. T. Nguyen, "The impact of cold waves and heat waves on mortality: evidence from a lower middle-income country," *Health Economics*, vol. 32, no. 6, pp. 1220–1243, 2023.

[9] J. Simister and C. Cooper, "Thermal stress in the U.S.A.: effects on violence and on employee behaviour," *Stress and Health*, vol. 21, no. 1, pp. 3–15, 2005.

[10] Z. Hao, A. AghaKouchak, and T. J. Phillips, "Changes in concurrent monthly precipitation and temperature extremes," *Environmental Research Letters*, vol. 8, no. 3, Article ID 34014, 2013.

[11] B. Lyon, "Southern Africa summer drought and heat waves: observations and coupled model behavior," *Journal of Climate*, vol. 22, no. 22, pp. 6033–6046, 2009.

[12] Bureau of Meteorology, "A prolonged autumn heatwave for southeast Australia," *Bureau of Meteorology Special Climate Statement*, vol. 45, 2013, http://www.bom.gov.au/climate/current/statements/scs45pdf.

[13] S. C. Lewis and D. J. Karoly, "Anthropogenic contributions to Australia's record summer temperatures of 2013," *Geophysical Research Letters*, vol. 40, no. 14, pp. 3705–3709, 2013.

[14] L. Tryhorn and J. Risbey, "On the distribution of heat waves over the Australian region," *Australian Meteorological Magazine*, vol. 55, no. 3, pp. 169–182, 2006.

[15] K. A. Bumbaco, K. D. Dello, and N. A. Bond, "History of Pacific Northwest heat waves: Synoptic pattern and trends," *Journal of Applied Meteorology and Climatology*, vol. 52, no. 7, pp. 1618–1631, 2013.

[16] Z. Wu, H. Lin, J. Li, Z. Jiang, and T. Ma, "Heat wave frequency variability over North America: Two distinct leading modes," *Journal of Geophysical Research: Atmospheres*, vol. 117, no. 2, 2012.

[17] M. D. Mastrandrea, C. Tebaldi, C. W. Snyder, and S. H. Schneider, "Current and future impacts of extreme events in California," *Climatic Change*, vol. 109, no. 1, pp. 43–70, 2011.

[18] K. E. Trenberth and J. T. Fasullo, "Climate extremes and climate change: The Russian heat wave and other climate extremes of 2010," *Journal of Geophysical Research: Atmospheres*, vol. 117, no. 17, 2012.

[19] D. Barriopedro, E. M. Fischer, J. Luterbacher, R. M. Trigo, and R. García-Herrera, "The hot summer of 2010: redrawing the temperature record map of Europe," *Science*, vol. 332, no. 6026, pp. 220–224, 2011.

[20] Z. Wu, Z. Jiang, J. Li, S. Zhong, and L. Wang, "Possible association of the western Tibetan Plateau snow cover with the decadal to interdecadal variations of northern China heatwave frequency," *Climate Dynamics*, vol. 39, no. 9-10, pp. 2393–2402, 2012.

[21] Y. Ding, G. Ren, Z. Zhao et al., "Detection, causes and projection of climate change over China: An overview of recent progress," *Advances in Atmospheric Sciences*, vol. 24, no. 6, pp. 954–971, 2007.

[22] E. M. Fischer and C. Schär, "Consistent geographical patterns of changes in high-impact European heatwaves," *Nature Geoscience*, vol. 3, no. 6, pp. 398–403, 2010.

[23] A. F. Carril, S. Gualdi, A. Cherchi, and A. Navarra, "Heatwaves in Europe: areas of homogeneous variability and links with the regional to large-scale atmospheric and SSTs anomalies," *Climate Dynamics*, vol. 30, no. 1, pp. 77–98, 2007.

[24] P. M. Della-Marta, J. Luterbacher, H. von Weissenfluh, E. Xoplaki, M. Brunet, and H. Wanner, "Summer heat waves over western Europe 1880–2003, their relationship to large-scale forcings and predictability," *Climate Dynamics*, vol. 29, no. 2-3, pp. 251–275, 2007.

[25] R. M. Trigo, R. García-Herrera, J. Díaz, I. F. Trigo, and M. A. Valente, "How exceptional was the early August 2003 heatwave in France?" *Geophysical Research Letters*, vol. 32, no. 10, Article ID 10701, 2005.

[26] Nchmf, *Vietnam Hydrology Meteorology Characteristics in 2019*, National Center for Hydro-Meteorological Forecasting Vietnam, Hanoi, Vietnam, 2019.

[27] R. Grotjahn, R. Black, R. Leung et al., "North American extreme temperature events and related large scale meteorological patterns: a review of statistical methods, dynamics, modeling, and trends," *Climate Dynamics*, vol. 46, no. 3-4, pp. 1151–1184, 2016.

[28] R.-Y. Lu and R.-D. Chen, "A review of recent studies on extreme heat in China," *Atmospheric and Oceanic Science Letters*, vol. 9, no. 2, pp. 114–121, 2016.

[29] K. Ward, S. Lauf, B. Kleinschmit, and W. Endlicher, "Heat waves and urban heat islands in Europe: A review of relevant drivers," *Science of the Total Environment*, vol. 569-570, pp. 527–539, 2016.

[30] M. Luo and N.-C. Lau, "Heat waves in southern China: Synoptic behavior, long-term change, and urbanization effects," *Journal of Climate*, vol. 30, no. 2, pp. 703–720, 2017.

[31] K. Hu, G. Huang, and R. Wu, "A strengthened influence of ENSO on August high temperature extremes over the southern Yangtze River valley since the late 1980s," *Journal of Climate*, vol. 26, no. 7, pp. 2205–2221, 2013.

[32] C. Tebaldi, K. Hayhoe, J. M. Arblaster, and G. A. Meehl, "Erratum: Going to the extremes-An intercomparison of model-simulated historical and future changes in extreme events," *Climatic Change*, vol. 79, pp. 185–234, 2006.

[33] K. E. Kunkel, X.-Z. Liang, and J. Zhu, "Regional climate model projections and uncertainties of US summer heat waves," *Journal of Climate*, vol. 23, no. 16, pp. 4447–4458, 2010.

[34] J. Kenyon and G. C. Hegerl, "Influence of modes of climate variability on global temperature extremes," *Journal of Climate*, vol. 21, no. 15, pp. 3872–3889, 2008.

[35] K. Guirguis, A. Gershunov, R. Schwartz, and S. Bennett, "Recent warm and cold daily winter temperature extremes in the Northern Hemisphere," *Geophysical Research Letters*, vol. 38, no. 17, 2011.

[36] C. J. White, D. Hudson, and O. Alves, "ENSO, the IOD and the intraseasonal prediction of heat extremes across Australia using POAMA-2," *Climate Dynamics*, vol. 43, no. 7-8, pp. 1791–1810, 2014.

[37] R. Chen, Z. Wen, and R. Lu, "Large-scale circulation anomalies and intraseasonal oscillations associated with long-lived extreme heat events in South China," *Journal of Climate*, vol. 31, no. 1, pp. 213–232, 2018.

[38] K. Hu, G. Huang, and R. Huang, "The impact of tropical Indian Ocean variability on summer surface air temperature in China," *Journal of Climate*, vol. 24, no. 20, pp. 5365–5377, 2011.

[39] R. Huang, J. Chen, L. Wang, and Z. Lin, "Characteristics, processes, and causes of the spatio-temporal variabilities of the East Asian monsoon system," *Advances in Atmospheric Sciences*, vol. 29, no. 5, pp. 910–942, 2012.

[40] P. C. Loikith and A. J. Broccoli, "Characteristics of observed atmospheric circulation patterns associated with temperature extremes over North America," *Journal of Climate*, vol. 25, no. 20, pp. 7266–7281, 2012.

[41] J. Wang, Z. Yan, X.-W. Quan, and J. Feng, "Urban warming in the 2013 summer heat wave in eastern China," *Climate Dynamics*, vol. 48, no. 9-10, pp. 3015–3033, 2017.

[42] L. Brunner, G. C. Hegerl, and A. K. Steiner, "Connecting atmospheric blocking to European temperature extremes in spring," *Journal of Climate*, vol. 30, no. 2, pp. 585–594, 2017.

[43] M. Luo and N.-C. Lau, "Synoptic characteristics, atmospheric controls, and long-term changes of heat waves over the Indochina Peninsula," *Climate Dynamics*, vol. 51, no. 7-8, pp. 2707–2723, 2018.

[44] L. Lin, C. Chen, and M. Luo, "Impacts of El Niño–Southern Oscillation on heat waves in the Indochina peninsula," *Atmospheric Science Letters*, vol. 19, no. 11, p. e856, 2018.

[45] N. Pham and T. Phan, *Climate of Vietnam*, Science and Technics Publishing house, Hanoi, Vietnam, 1993.

[46] U. N. E. Programme, *Vietnam Assessment Report on Climate Change*, United Nations Environment Programme, Nairobi, Kenya, 2009, https://wedocs.unep.org/xmlui/handle/20.500.11822/7940.

[47] V.-T. Phan, T. Ngo-Duc, and T. Ho, "Seasonal and interannual variations of surface climate elements over Vietnam," *Climate Research*, vol. 40, no. 1, pp. 49–60, 2009.

[48] P. Q. Ha, "Carbon in Vietnamese soils and experiences to improve carbon stock in soil," in *Proceedings of the International Workshop on Evaluation and Sustainable Management of Soil Carbon Sequestration in Asian Countries*, pp. 28-29, Bogor, Indonesia, September 2010.

[49] V. T. Phuong, "Forest environment of Vietnam: features of forest vegetation and soils," in *Forest Environments in the Mekong River Basin*, pp. 189–200, Springer, Berlin, Germany, 2007.

[50] B. Abidoye, T. Truong, P. Kurukulasuriya, R. Mendelsohn, M. Tomova, and R. Dobias, *Economics of Climate Change Adaptation: Agriculture Sector Analysis for Viet Nam*, United States Agency for International Development, Washington, DC, USA, 2016.

[51] Ministry of Agriculture and Rural Development, *Announcement of National forest Status in 2021 (2860/QĐ-BNN-TCLN)*, Information technology laws, Hanoi, Vietnam, 2022.

[52] N. N. Lung, N. X. Quat, and T. V. Lien, *Final Report on forest Ecological Stratification in Vietnam*, UN-REDD Program Vietnam, Hanoi, Vietnam, 2011.

[53] E. Kalnay, M. Kanamitsu, R. Kistler et al., "The NCEP/NCAR 40-year reanalysis project," *Bulletin of the American Meteorological Society*, vol. 77, no. 3, pp. 437–471, 1996.

[54] T. Foken, M. Göockede, M. Mauder, L. Mahrt, B. Amiro, and W. Munger, "Post-field data quality control," in *Handbook of Micrometeorology: A Guide for Surface Flux Measurement and Analysis*, pp. 181–208, Springer, Berlin, Germany, 2004.

[55] N.-C. Lau and M. J. Nath, "Model simulation and projection of European heat waves in present-day and future climates," *Journal of Climate*, vol. 27, no. 10, pp. 3713–3730, 2014.

[56] T. T. Smith, B. F. Zaitchik, and J. M. Gohlke, "Heat waves in the United States: definitions, patterns and trends," *Climatic Change*, vol. 118, no. 3-4, pp. 811–825, 2013.

[57] H. Teng, G. Branstator, H. Wang, G. A. Meehl, and W. M. Washington, "Probability of US heat waves affected by a subseasonal planetary wave pattern," *Nature Geoscience*, vol. 6, no. 12, pp. 1056–1061, 2013.

[58] M. Gao, B. Wang, J. Yang, and W. Dong, "Are peak summer sultry heat wave days over the Yangtze–Huaihe River basin predictable?" *Journal of Climate*, vol. 31, no. 6, pp. 2185–2196, 2018.

[59] D. S. Wilks, *Statistical Methods In The Atmospheric Sciences*, Elsevier, Amsterdam, The Netherlands, 2006.

[60] T. Phan-Van, P. Nguyen-Ngoc-Bich, T. Ngo-Duc et al., "Drought over Southeast Asia and its association with large-scale drivers," *Journal of Climate*, vol. 35, no. 15, pp. 4959–4978, 2022.

[61] P. K. Sen, "Estimates of the regression coefficient based on Kendall's tau," *Journal of the American Statistical Association*, vol. 63, no. 324, pp. 1379–1389, 1968.

[62] H. B. Mann, "Nonparametric tests against trend," *Econometrica*, vol. 13, no. 3, pp. 245–259, 1945.

[63] M. G. Kendall, *Rank Correlation Methods*, Charles Griffin and Company, London, UK, 2 edition, 1955.

[64] C. Chou, J.-Y. Tu, and J.-Y. Yu, "Interannual variability of the western North Pacific summer monsoon: Differences between ENSO and non-ENSO years," *Journal of Climate*, vol. 16, no. 13, pp. 2275–2287, 2003.

[65] C. Li, R. Lu, and B. Dong, "Predictability of the western North Pacific summer climate associated with different ENSO phases by ENSEMBLES multi-model seasonal forecasts," *Climate Dynamics*, vol. 43, no. 7-8, pp. 1829–1845, 2014.

[66] D. Nguyen, J. Renwick, and J. McGregor, "Variations of surface temperature and rainfall in Vietnam from 1971 to 2010," *International Journal of Climatology*, vol. 34, no. 1, pp. 249–264, 2014.

[67] B. Wang and Q. Zhang, "Pacific–east Asian teleconnection. Part II: How the Philippine Sea anomalous anticyclone is established during El Nino development," *Journal of Climate*, vol. 15, no. 22, pp. 3252–3265, 2002.

[68] N.-C. Lau and M. J. Nath, "Atmosphere–ocean variations in the Indo-Pacific sector during ENSO episodes," *Journal of Climate*, vol. 16, no. 1, pp. 3–20, 2003.